*Q. J. R. Meteorol. Soc.* (1997), **123**, pp. 929–951

# The zonal momentum balance in an eddy-resolving general-circulation model of the Southern Ocean

By DAVID P. STEVENS[1]* and VLADIMIR O. IVCHENKO[2]
[1]*University of East Anglia, UK*
[2]*Southampton University, UK*

(Received 21 December 1995; revised 26 July 1996)

SUMMARY

The momentum balance in the zonally unbounded region of the Southern Ocean is examined using an eddy-resolving ocean general-circulation model (namely FRAM). Momentum, which is input at the surface and accelerates the Antarctic Circumpolar Current, is transferred down the water column and removed by topographic form stress. Bottom friction and lateral eddy viscosity are found to be negligible. The poleward flux of eastward momentum has a small effect in redistributing momentum. In spite of this, below the wind-driven surface layer and above the level of topography, the poleward momentum-flux divergence provides the main balance along with the ageostrophic flux of planetary vorticity (although the magnitude of these terms is an order of magnitude smaller than the wind stress). Below the Ekman layer, standing eddies produce a drag on the flow whilst transient eddies accelerate the flow. However, the impact of transient eddies is smaller. The downward transfer of momentum is achieved by interfacial form stress. This can be understood in terms of a poleward density (heat) flux. The main contribution comes from standing eddies, with a smaller contribution from transient eddies. Both contributions assist the transfer. The flux of density (heat) from the neighbouring oceans (to the north and south of the Drake Passage latitudes) influences the depth penetration of zonal momentum, particularly in the upper 1000 m. The Johnson–Bryden theory is generalized to give an additional term which is proportional to the stream function for the residual circulation associated with Eliassen–Palm cross-sections.

## 1. INTRODUCTION

The Southern Ocean is the only region in the world ocean where a zonally unbounded current exists. As such the Antarctic Circumpolar Current (ACC) is of significant dynamical interest. The almost constant eastward wind stress accelerates this current. There may also be a significant amount of driving by buoyancy forcing (Cox 1990; Olbers and Wübber 1991), however this is not directly considered here. There have been a number of attempts at modelling and understanding the ACC. Nowlin and Klinck (1986) provide a comprehensive review of the physics of the ACC. More recently the article of Johnson and Bryden (1989) included a neat overview.

The ACC has featured in a number of primitive-equation models starting with Gill and Bryan (1971). They used an idealized geometry, zonal winds and an imposed surface-temperature distribution. The transport in the ACC increased when a topographic barrier was introduced. This was due to the pressure difference across the topography, which accelerated the flow. The ACC is included in a number of world ocean models such as Bryan and Cox (1972), Bye and Sag (1972), Cox (1975), Bryan *et al.* (1975), Cox (1990) and Manabe *et al.* (1990). All of these models (by necessity) had coarse finite-difference grids. This leads to large eddy viscosities and a poor (if any) representation of topography. Thus the reality of the dynamics of the ACC in these models must be in some doubt.

Much of the modelling of the ACC has utilized quasi-geostrophic models. McWilliams *et al.* (1978) created a two-layer eddy-resolving model of a wind-driven flow in a zonal channel (sometimes with partial meridional barriers) on a $\beta$-plane. In these experiments transient eddies play an important role. The eddies are generated by baroclinic and barotropic instability of the mean flow. The lateral Reynolds stress exerted by these eddies on the mean flow tends to transfer zonal momentum into the centre of the jet. The mechanism for the downward transfer of the zonal momentum is interfacial form stress. The interfacial form stress is produced by transient eddies, or by standing eddies (or both). It is important

* Corresponding author: School of Mathematics, University of East Anglia, Norwich, NR4 7TJ, UK.

to note that this mechanism is inviscid. In their experiment with flat-bottom topography, standing eddies and topographic form stress are absent and the transport of the ACC is more than 800 Sverdrups. In the experiment with a topographic obstacle and partial meridional barriers, interfacial form stress is important for the downward momentum transfer. In this case topographic form stress provides the sink of the zonal momentum. Interfacial and topographic form stresses depend more on standing eddies than on transient eddies. The volume transport of the ACC in this experiment is reduced to less than 100 Sverdrups.

McWilliams and Chow (1981) continued eddy-resolving experiments using a 3-layer flat-bottom zonal channel quasi-geostrophic model. They found a strong meandering eastward flow. There is concentration of momentum toward the middle of the channel in all layers. However, this is much stronger in the upper layer than in the lower layer. Both the mean flow and the eddies are quite weak near the northern and southern boundaries, where wind stress reduces to zero. This means that the boundaries do not affect the solution very much.

Wolff *et al.* (1991) discuss the results of a number of eddy-resolving numerical experiments with different topographic obstacles. The relative contribution of transient or standing eddies to the interfacial form stress depends first of all on the position of the topographic obstacles in the channel and on the magnitude of the bottom friction. Topographic form stress is the main sink of zonal momentum (if bottom friction is not too big and also if the main topographic obstacles are not too far from latitudes where the wind is a maximum).

Treguier and McWilliams (1990) showed that an isolated topographical feature in the path of a jet is more important for momentum balance than a randomly distributed topography for the same root-mean-square height. The topographic form stress can not only remove the eastward momentum, but even force counter currents.

Marshall (1995) examined the influence of topography on the ACC using an analytic model. He found that the flow in the upper 3 km of the water column was near zonal in the limit of minimal bottom currents. However, on increasing the strength of the bottom velocities the path of the current tended toward $f/H$ contours, where $f$ is the Coriolis parameter and $H$ is the depth.

For a good description of the ACC it is necessary to have a high spatial resolution. Semtner and Chervin (1988, 1992) have run a world ocean model at high resolution (0.5° in latitude and logitude). However, little analysis of the ACC has been attempted. The UK community have run FRAM (Fine-Resolution Antarctic Model). This model is described in the next section. FRAM allows analysis of the velocity, temperature, and salinity fields at high resolution. Thus it may be possible to answer some unresolved questions using FRAM results. These questions are:

- What is the zonal momentum balance in the ACC belt (ACCB)? (The ACCB is the area around Antarctica at the latitudes of the Drake Passage.) How does the momentum balance change with depth? Even quite recent papers (Johnson and Bryden 1989; Wolff *et al.* 1991) mention that there is uncertainty and debate over the exact mechanisms of momentum transfer and dissipation.
- What effect do the surrounding oceans have on the dynamics of the ACC? How does this influence relate to the penetration of the zonal momentum and what is the mechanism? Models of flow in a zonal channel with solid boundaries do not describe this influence. Most models of the world ocean models do not have enough spatial resolution. Marshall *et al.* (1993) use results from a quasi-geostrophic model for the circumpolar flow around Antarctica. They find good agreement with the Johnsonand

Bryden (1989) theory, in which the zonal momentum input by the wind is transferred downwards by interfacial form stress associated with meridional density fluxes.

- What is the relative importance of transient and standing eddies in the dynamics of the ACCB? Because of the influence of topography the main jets of the ACC have large meridional displacements. In many places the ACC moves away (more often to the north) from the ACCB. Thus it should be expected that standing eddies are important.

It is also of interest to examine the structure of the ACC in a streamwise coordinate frame. Such an approach is considered by Ivchenko *et al.* (1996).

## 2. The model

The UK FRAM project is a community research program whose aim is a detailed study of the Southern Ocean. Central to this study is an eddy-resolving ocean general-circulation model, based on that of Cox (1984). In the spherical coordinate system used by the model, the equations of motion are

$$\frac{\partial u}{\partial t} + \Gamma(u) - fv = -\frac{1}{\rho_0 a \cos\phi}\frac{\partial p}{\partial \lambda} + K_m \frac{\partial^2 u}{\partial z^2} + F^u, \tag{1}$$

$$\frac{\partial v}{\partial t} + \Gamma(v) + fu = -\frac{1}{\rho_0 a}\frac{\partial p}{\partial \phi} + K_m \frac{\partial^2 v}{\partial z^2} + F^v, \tag{2}$$

$$\frac{\partial p}{\partial z} = -\rho g, \tag{3}$$

$$\Gamma(1) = 0, \tag{4}$$

$$\frac{\partial T}{\partial t} + \Gamma(T) = K_h \frac{\partial^2 T}{\partial z^2} + A_h \nabla^2 T - B_h \nabla^4 T, \tag{5}$$

$$\rho = \rho(\theta, S, z), \tag{6}$$

where

$$\Gamma(\mu) = \frac{1}{a\cos\phi}\frac{\partial}{\partial\lambda}(u\mu) + \frac{1}{a\cos\phi}\frac{\partial}{\partial\phi}(v\mu\cos\phi) + \frac{\partial}{\partial z}(w\mu),$$

$$F^u = A_m\left(\nabla^2 u + \frac{(1-\tan^2\phi)u}{a^2} - \frac{2\sin\phi}{a^2\cos^2\phi}\frac{\partial v}{\partial\lambda}\right) - B_m\nabla^4 u,$$

$$F^v = A_m\left(\nabla^2 v + \frac{(1-\tan^2\phi)v}{a^2} + \frac{2\sin\phi}{a^2\cos^2\phi}\frac{\partial u}{\partial\lambda}\right) - B_m\nabla^4 v,$$

$$\nabla^2(\mu) = \frac{1}{a^2\cos^2\phi}\frac{\partial^2\mu}{\partial\lambda^2} + \frac{1}{a^2\cos\phi}\frac{\partial}{\partial\phi}\left(\frac{\partial\mu}{\partial\phi}\cos\phi\right).$$

The variables $\phi$, $\lambda$, $z$, $t$, $u$, $v$, $w$, $p$ represent latitude, longitude, depth, time, zonal velocity, meridional velocity, vertical velocity and pressure respectively. The radius of the earth is $a$, $g$ is the acceleration due to gravity, and $f = 2\Omega\sin\phi$ is the Coriolis parameter, where $\Omega$ is the speed of angular rotation of the earth. The variable $T$ represents tracers such as potential temperature, $\theta$, and salinity, $S$. The density, $\rho$, is given by theequation of

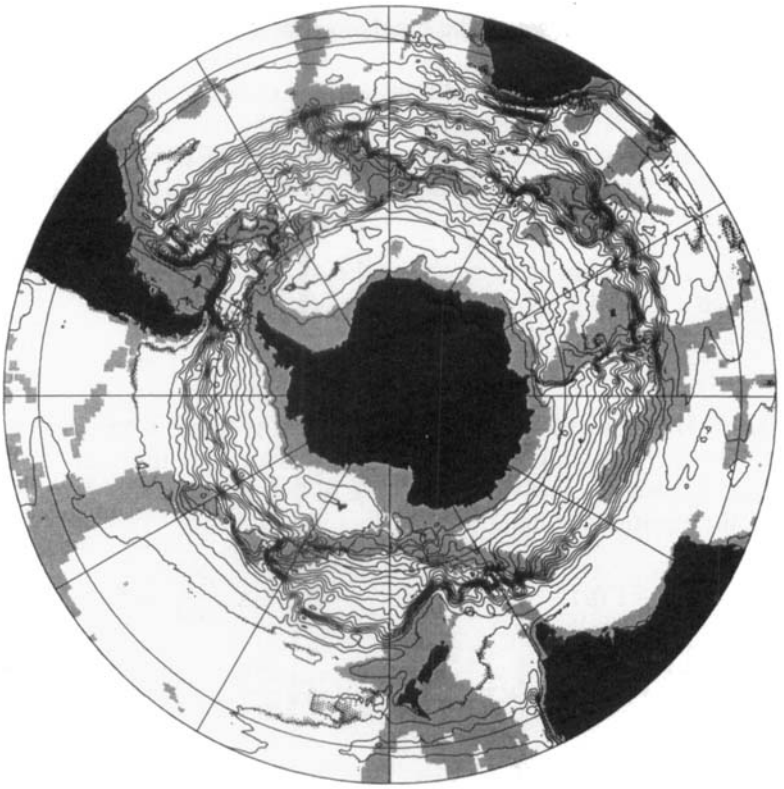

Figure 1. The time-mean mass transport stream function. The contour interval is 10 Sverdrups. Major topographic features (with a depth of less than 3000 m) are represented by shading.

state (6) and $\rho_0$ is a reference density. Horizontal mixing is by a combination of harmonic and bi-harmonic operators. $A_m$ and $B_m$ are the mixing coefficients for momentum and $A_h$ and $B_h$ are the mixing coefficients for tracers. The coefficients of vertical mixing are $K_m$ and $K_h$ for momentum and tracers respectively.

The model was spun-up over six years using the Levitus (1982) temperature and salinity climatology, and Hellerman and Rosenstein (1983) wind stresses. Further details of the model and results from this period of the integration can be found in the article by the FRAM group (1991) and in the atlas produced by Webb *et al.* (1991). The integration was continued for a further ten years, with the final six years as an analysis phase. During this phase the eddy kinetic-energy field produced by FRAM compares reasonably well with observations from drifting buoys and satellite altimetry (Stevens and Killworth 1992). Analysis of such a large model is a major task. Others (heat and freshwater fluxes by Saunders and Thompson (1993), vorticity budget by Wells and de Cuevas (1995), momentum balance on density coordinates by Killworth and Nanneh (1994), meridional circulation by Döös and Webb (1994)) have analysed other components of the model.

The model appears to reproduce many of the known features in the Southern Ocean extremely well. Figure 1 illustrates contours of the mean mass transport stream function during the final six years of the integration. There is a great deal of detail and structure. Many of the small narrow jets associated with the ACC can be seen. Topographic effects are dominant as can be seen from the 3000 m isobath (shallower regions are shaded). Much of the path of the ACC is displaced to the north of the latitude circles passing through

Drake Passage. One point of note is the transport through Drake Passage, which at 180 Sverdrups is higher than the generally recognised 120–130 Sverdrups (Nowlin and Klinck 1986). This overestimation of the transport in the ACC is endemic in primitive-equation models. For instance, the global eddy-resolving model of Semtner and Chervin (1988) has a transport of 190 Sverdrups through Drake Passage. Grose (1992) has shown that the International Southern Ocean studies (ISOS) current meter array would underestimate the transport through Drake Passage in FRAM. Some of the difference is due to the smoothed nature of topography in FRAM. However, this underestimate is not large enough to explain the difference between the observed and modelled transports.

The analysis presented here concentrates on the dynamics in the time and zonal average. It is therefore useful to look at the averaged dynamical fields. Figure 2(a) shows the time and zonally averaged eastward velocity. The broad nature of the eastward current in the zonal average is apparent. However, individual meridional sections show (Webb *et al.* 1991) that the current is made up of a number of narrow jets with relatively small vertical shear. At depth there is some reversal of the zonally averaged current. This has been noted in the inverse study of Olbers and Wenzel (1990), which used the hydrographic atlas prepared by Gordon *et al.* (1982).

The time-mean zonally averaged meridional overturning is depicted in Fig. 2(b). The zonally unbounded region is also illustrated. The picture is dominated by the so called 'Deacon Cell' (Döös and Webb 1994), which lies between 60°S and 30°S. There is no observational evidence for this cell; however, such a cell occurs in many other primitive-equation models (Semtner and Chervin 1988; Manabe *et al.* 1990). Using a coarse-resolution global model, Danabasoglu *et al.* (1994) found that the cell vanished when they added a parametrized eddy-induced transport velocity to the mean velocity. Below the Deacon Cell there is a southward current which enters the model at its northern boundary and returns northwards at great depth. There is little deep-water formation. This is because the model has annual mean surface buoyancy forcing. Thus the wintertime conditions which are required for deep-water formation are not attained. It is quite likely that the deep northward flow would be connected to the surface by a region of bottom-water formation if such conditions existed. A simulation with full seasonally varying buoyancy fluxes and a sea-ice model was initiated, but later abandoned due to a lack of computer resources.

## 3. The depth-integrated zonal momentum balance

The time-mean, zonally averaged and depth-integrated form of (1), the zonal (or eastward) momentum balance, can be written as

$$\rho_0\overline{\left[\int_{-H}^{0}\frac{\partial u}{\partial t}\,\mathrm{d}z\right]}+\rho_0\overline{\left[\frac{1}{a\cos\phi}\frac{\partial}{\partial\phi}\int_{-H}^{0}uv\cos\phi\,\mathrm{d}z\right]}=$$

$$-\frac{1}{a\cos\phi}\overline{\left[H\frac{\partial p_s}{\partial\lambda}+\int_{-H}^{0}\int_{z}^{0}g\frac{\partial\rho}{\partial\lambda}\,\mathrm{d}z'\,\mathrm{d}z\right]}+\overline{[\tau_s^\lambda]}-\overline{[\tau_b^\lambda]}+\rho_0\overline{\left[\int_{-H}^{0}F^u\,\mathrm{d}z\right]}. \quad (7)$$

The variables $p_s$, $\tau_s^\lambda$, $\tau_b^\lambda$ represent surface pressure, zonal wind stress and zonal bottom stress respectively. The square bracket represents a zonal average and an overbar denotes a time average. The Coriolis term $-fv$ of (1) vanishes in (7) because of mass conservation. It is worth noting that if the depth $H$ were constant in (7) then the form drag (pressure term) would make no contribution.

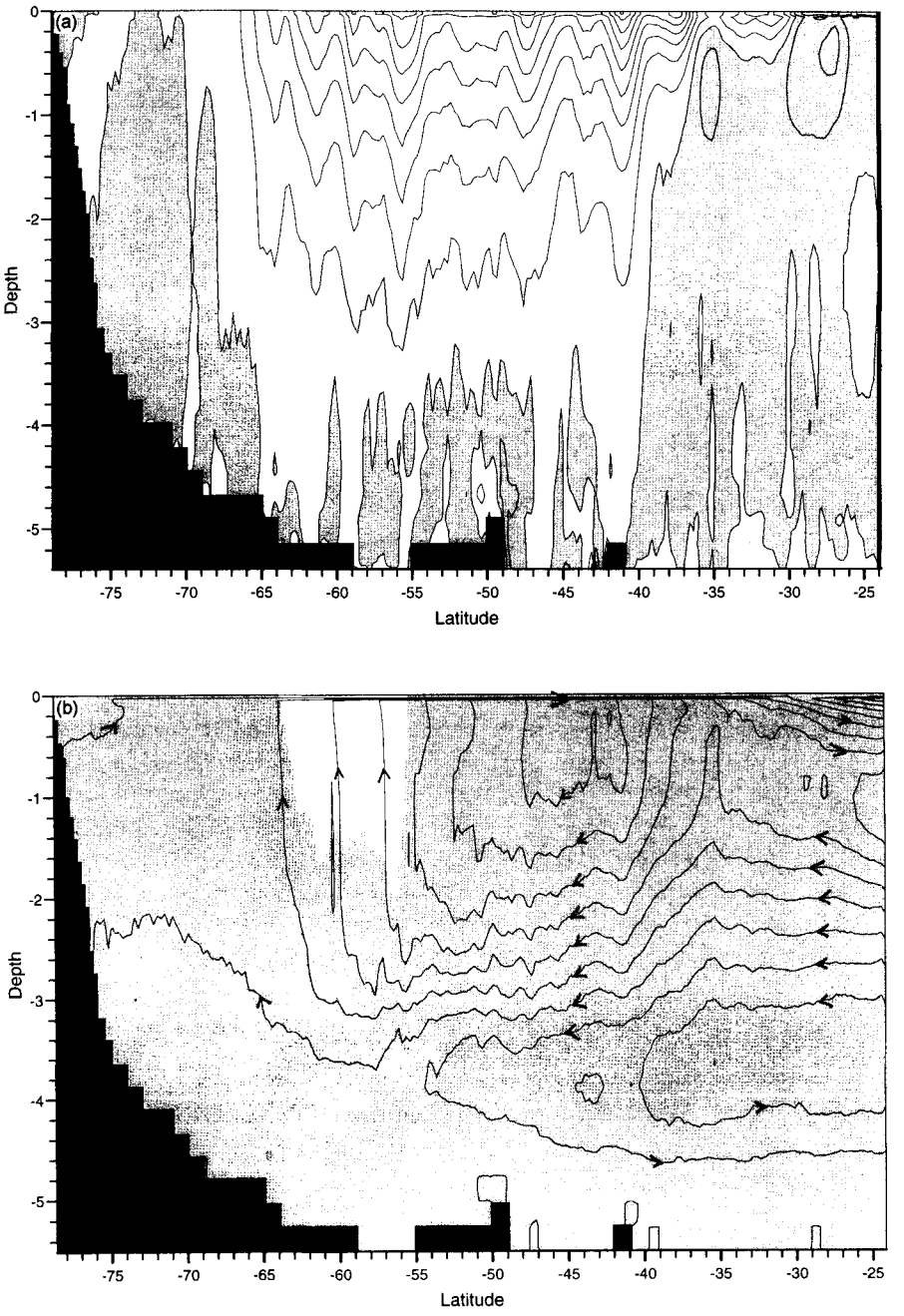


Figure 2. (a) The time-mean zonally averaged eastward velocity, westward flow is shaded. The contour interval is 0.01 m $s^{-1}$ and the depth is in km. (b) The time-mean zonally integrated meridional overturning. The contour interval is 5 Sverdrups and the depth is in km. The unshaded region is zonally unbounded.

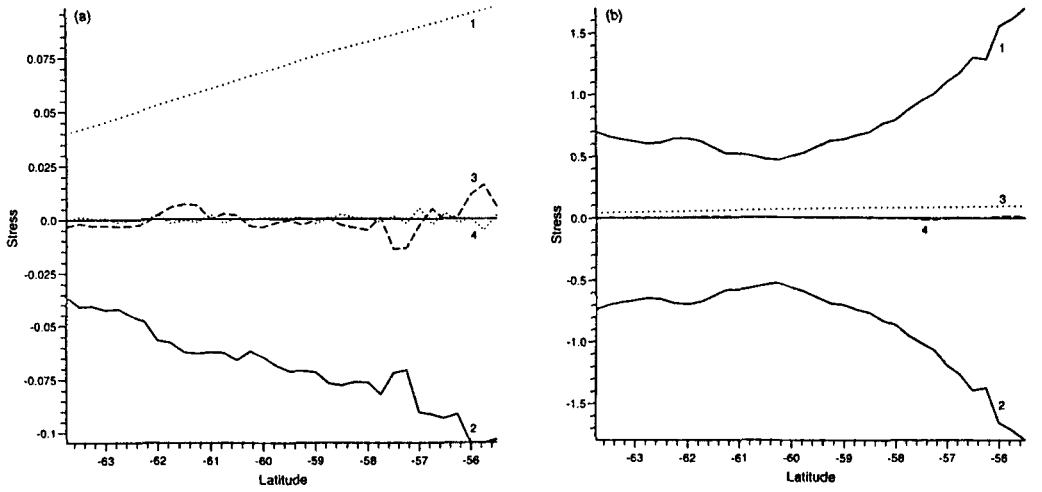


Figure 3. (a) The depth-integrated, time and zonally averaged momentum balance. Lines 1, 2, 3 and 4 represent the zonal wind stress, bottom form drag, poleward momentum-flux divergence, and remaining (small) terms respectively. (b) As (a) but with the two components of the pressure term considered separately. Lines 1, 2, 3 and 4 represent the hydrostatic pressure, surface pressure, wind stress and poleward momentum-flux divergence terms respectively. The units of stress are N $m^{-2}$.

The individual terms in (7) are diagnosed from FRAM for the latitude circles which pass through Drake Passage. Figure 3(a) shows the balance taken over the final two years of the 16-year model run. These results were produced as the model was running and included data from one time-step from each model day. The same analysis has been carried out with 72 monthly model dumps, from the final six years of the model run, with indistinguishable results. To leading order a much simpler balance holds, namely

$$\rho_0\overline{\left[\frac{1}{a\cos\phi}\frac{\partial}{\partial\phi}\int_{-H}^{0} uv\cos\phi\,\mathrm{d}z\right]} = -\frac{1}{a\cos\phi}\overline{\left[H\frac{\partial p_s}{\partial\lambda}+\int_{-H}^{0}\int_{z}^{0} g\frac{\partial\rho}{\partial\lambda}\,\mathrm{d}z'\,\mathrm{d}z\right]}+\overline{[\tau_s^{\lambda}]}. \tag{8}$$

In this equation the surface eastward wind stress is balanced almost entirely by bottom form stress, with only a small contribution coming from the poleward momentum-flux divergence. Killworth and Nanneh (1994) also found the poleward momentum-flux divergence to be consistently small in their isopycnal momentum budget. The bottom form stress is an inviscid mechanism, in which horizontal pressure gradients redistribute zonal and meridional momentum. Bottom friction and lateral viscosity are much smaller than bottom form stress in FRAM.

The balance between the surface wind stress and the bottom form stress has been suspected for a long time (Munk and Palmén 1951). More recently Johnson and Bryden (1989) reviewed a number of calculations of the poleward momentum flux. These all showed that it was at least an order of magnitude too small to balance the wind stress. They thus concluded that the wind stress must be balanced primarily by bottom form stress. Another recent study by Morrow *et al.* (1992) used GEOSAT data to calculate the poleward momentum flux due to transient eddies. They found that the zonal average of the momentum flux was an order of magnitude too small and in the wrong direction to balance the momentum input by the wind.

It is also of interest to look at the balance achieved when the two components of the pressure term in (8) are considered separately (Fig. 3(b)). These terms are an order of

magnitude larger than the combined term. The part due to the surface pressure opposes the current. In a homogeneous ocean with topography, the surface-pressure term would balance the wind. Such simulations (Gill and Bryan 1971) have very low circumpolar transports. The second term, due to the hydrostatic pressure, accelerates the current. Therefore the stratification (and thus the baroclinic mode) is compensating for the barotropic mode. This mechanism has been discussed in more detail by Olbers and Wübber (1991).

## 4. The vertical structure of the zonal momentum balance

It is interesting to consider the vertical structure of the time-mean zonal momentum balance. Integrating (1) between any two depths $-h_a$ and $-h_b$ ($h_b > h_a$) and taking a time and zonal mean, the following balance holds

$$\overline{\rho_0\left[\int_{-h_b}^{-h_a} \frac{\partial u}{\partial t}\,dz\right]} + \overline{\rho_0\left[\int_{-h_b}^{-h_a} \frac{1}{a\cos\phi}\frac{\partial}{\partial\lambda}(u^2) + \frac{1}{a\cos\phi}\frac{\partial}{\partial\phi}(uv\cos\phi) + \frac{\partial}{\partial z}(uw)\,dz\right]}$$

$$-\overline{\rho_0\left[\int_{-h_b}^{-h_a} fv\,dz\right]} = -\frac{1}{a\cos\phi}\overline{\left[\int_{-h_b}^{-h_a} \frac{\partial p}{\partial\lambda}\,dz\right]}$$

$$+\overline{\rho_0\left[\int_{-h_b}^{-h_a} K_m\frac{\partial^2 u}{\partial z^2}\,dz\right]} + \overline{\rho_0\left[\int_{-h_b}^{-h_a} F^u\,dz\right]}. \tag{9}$$

The first term on the left-hand side of (9), the time rate of change, is negligible for a long time average. The zonal average of the divergence of the eastward flux of eastward momentum is identically zero. The pressure-gradient term is identically zero if $h_b$ is above the level which intersects topography ($h_T$).

The zonal momentum balance is split into seven parts to examine its vertical structure.

### (a) *The surface layer*

In FRAM the balance at the surface (Fig. 4) is almost exactly

$$-\overline{\rho_0\left[\int_{-h_E}^{0} fv\,dz\right]} = \overline{[\tau_s^\lambda]}, \tag{10}$$

where $h_E$ is the depth of the upper Ekman layer (this is taken to be 20.7 m, the thickness of the upper level of the model). Thus (10) states that the eastward momentum input at the surface by the wind produces a northward Ekman transport. The magnitude of this transport varies from 7 Sverdrups in the south of the ACCB to 17 Sverdrups in the north. In fact, the balance (10) has been shown (Döös and Webb 1994) to hold at all latitudes in FRAM.

### (b) *Intermediate depths*

Integrating over level 2 (20.7–44 m) immediately below the Ekman layer, the balance in FRAM is

$$\overline{\rho_0\left[\int_{-h_2}^{-h_E} \frac{1}{a\cos\phi}\frac{\partial}{\partial\phi}(uv\cos\phi)\,dz\right]} - \overline{\rho_0\left[\int_{-h_2}^{-h_E} fv\,dz\right]} = \overline{\rho_0\left[\int_{-h_2}^{-h_E} K_m\frac{\partial^2 u}{\partial z^2}\,dz\right]}, \tag{11}$$

where $h_2 = 44$ m. The relative size of each term can be seen in Fig. 5(a). The dominant terms are the poleward momentum-flux divergence (or the divergence of Reynolds stress

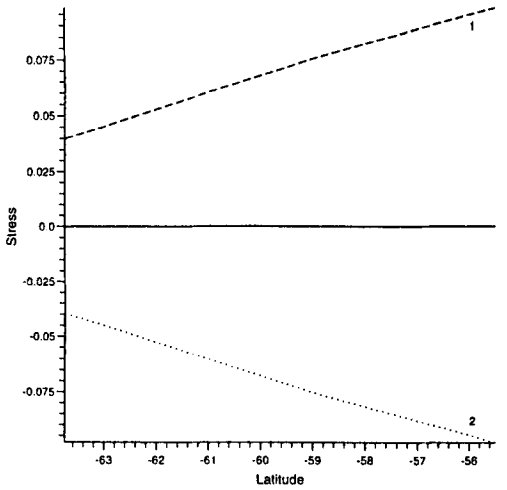


Figure 4. The time and zonally averaged momentum balance in the surface Ekman layer (0–20.7 m). Lines 1 and 2 represent the zonal wind stress and Coriolis terms respectively. The units of stress are N $m^{-2}$.

or meridional eddy relative vorticity flux) and the Coriolis term (or ageostrophic flux of planetary vorticity). There is also a small contribution from the vertical stress divergence. This is due to the large difference in velocity at the base of the Ekman layer. It is important to note that the magnitude of the terms here are at least an order smaller than those in Fig. 4. This because there are no large terms (pressure gradient or wind stress) to balance the Coriolis term. It should also be noted, as we will see in section 5(*a*), that the Coriolis term is the difference of two terms that are of the same order of magnitude as the wind stress. These terms are related to the interfacial form stress which is responsible for the vertical transfer of zonal momentum.

It is of interest to split the poleward momentum-flux term into its constituent parts, namely the mean, standing and transient components

$$\rho_0 \int_{-h_2}^{-h_E} \frac{1}{a \cos\phi} \frac{\partial}{\partial \phi} \left\{ \left( [\overline{u}]\,[\overline{v}] + [\overline{u_*}\,\overline{v_*}] + \overline{[u'v']} \right) \cos\phi \right\} \, dz.$$

In the above $_*$ denotes standing eddy components (that is deviations from the zonal mean) and $'$ denotes transient eddy components. Thus $v = v_* + [v]$ with $[v_*] = 0$ and $v = v' + \overline{v}$ with $\overline{v'} = 0$. The relative sizes of these terms at level 2 are illustrated in Fig. 5(b). The mean component (associated with the meridional circulation) is extremely small, as $\overline{[v]}$ is small in the ACCB (above the level of topographic obstacles). The magnitude of the standing component is approximately twice that of the transient component.

The mean zonal velocity in the ACCB is positive at most levels down to quite large depths. At large depths the zonal velocity can be negative, but is small in magnitude. In the top 2 km of the ACCB, profiles of the zonal velocity look similar for different levels (see Fig. 5(c)) and change only in the magnitude of the velocity. This feature of FRAM has been noted by Killworth (1992) and explained in terms of an equivalent-barotropic mode. Away from the surface Ekman layer, the characteristic scale of the mean zonal velocity decreases nearly linearly with depth. In the ACCB the mean zonal velocity increases equatorward (as does the wind stress). There are three peaks: at latitudes $\phi = 61.5°$S, $\phi = 59°$S and $\phi = 56°$S (see Fig. 5(c)). At approximately the same latitudes there are three peaks of the poleward momentum-flux divergence (see Fig. 5(b)). Places with a local minimum of the

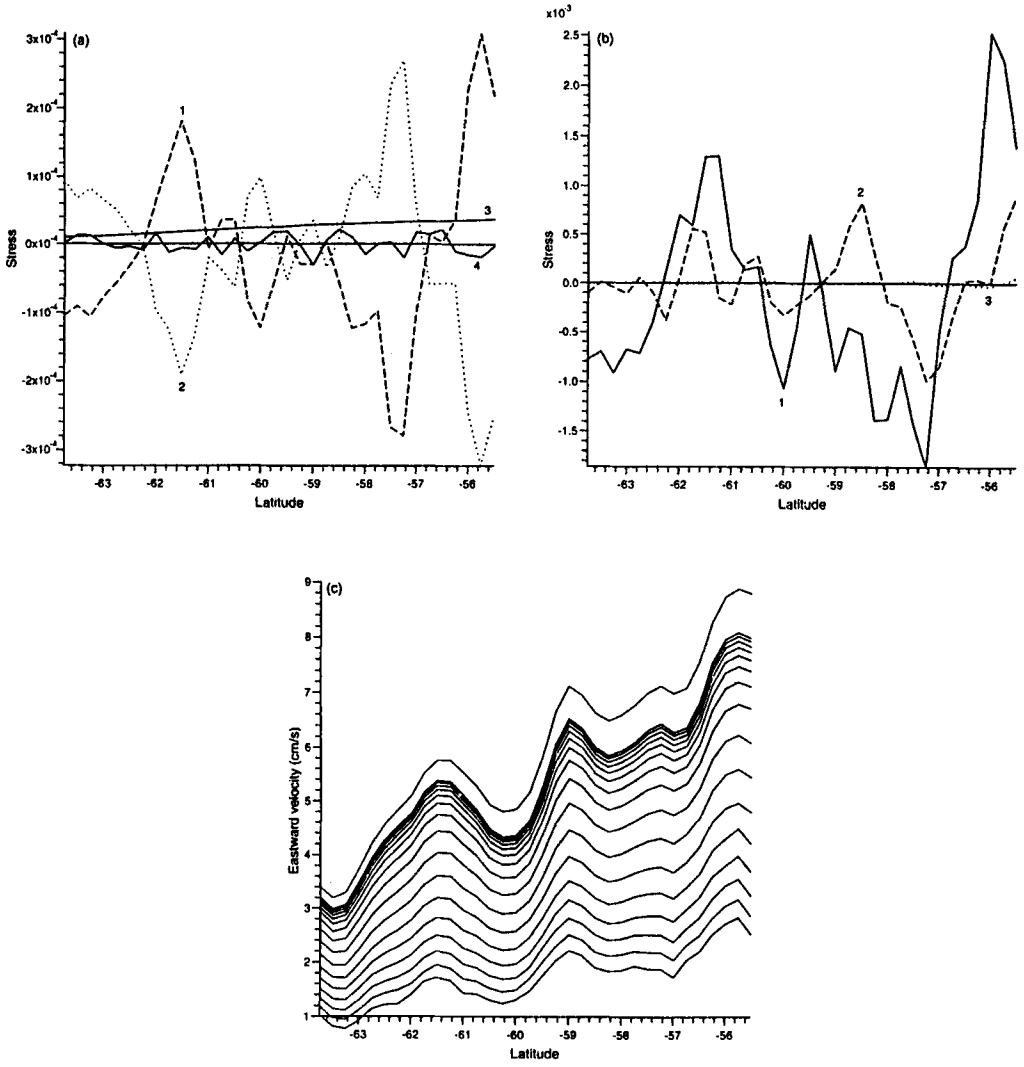


Figure 5. (a) The time and zonally averaged momentum balance at level 2 (20.7–44 m). Lines 1, 2, 3 and 4 represent the divergence of Reynolds stress, Coriolis, vertical momentum mixing and remaining (small) terms respectively. The units of stress are N $m^{-2}$. (b) The divergence of the Reynolds stress due to, 1 standing eddies, 2 transient eddies, and 3 the mean flow at level 2. The units of stress are N $m^{-2}$. (c) The average zonal velocity $\overline{[u]}$ at levels $k$=1–17 (0–2056 m). The velocity decreases monotonically with depth.

zonal velocity correspond to local minima of poleward momentum-flux divergence. Thus, standing and transient eddies redistribute zonal momentum horizontally, accelerating the flow in some regions, and decelerating it in others.

Above the base of level 6 ($h_6 = 185.5$ m) there is no zonal obstruction anywhere in the ACCB. The balance between $-h_2$ and $-h_6$ is

$$\overline{\rho_0\left[\int_{-h_6}^{-h_2} \frac{1}{a\cos\phi}\frac{\partial}{\partial\phi}(uv\cos\phi)\,\mathrm{d}z\right]} - \overline{\rho_0\left[\int_{-h_6}^{-h_2} fv\,\mathrm{d}z\right]} = 0. \tag{12}$$

As can be seen in Fig. 6(a) the structure is similar to that in Fig. 5(a) apart from the absence of the vertical-shear term. This is the main balance in the region below the wind-driven

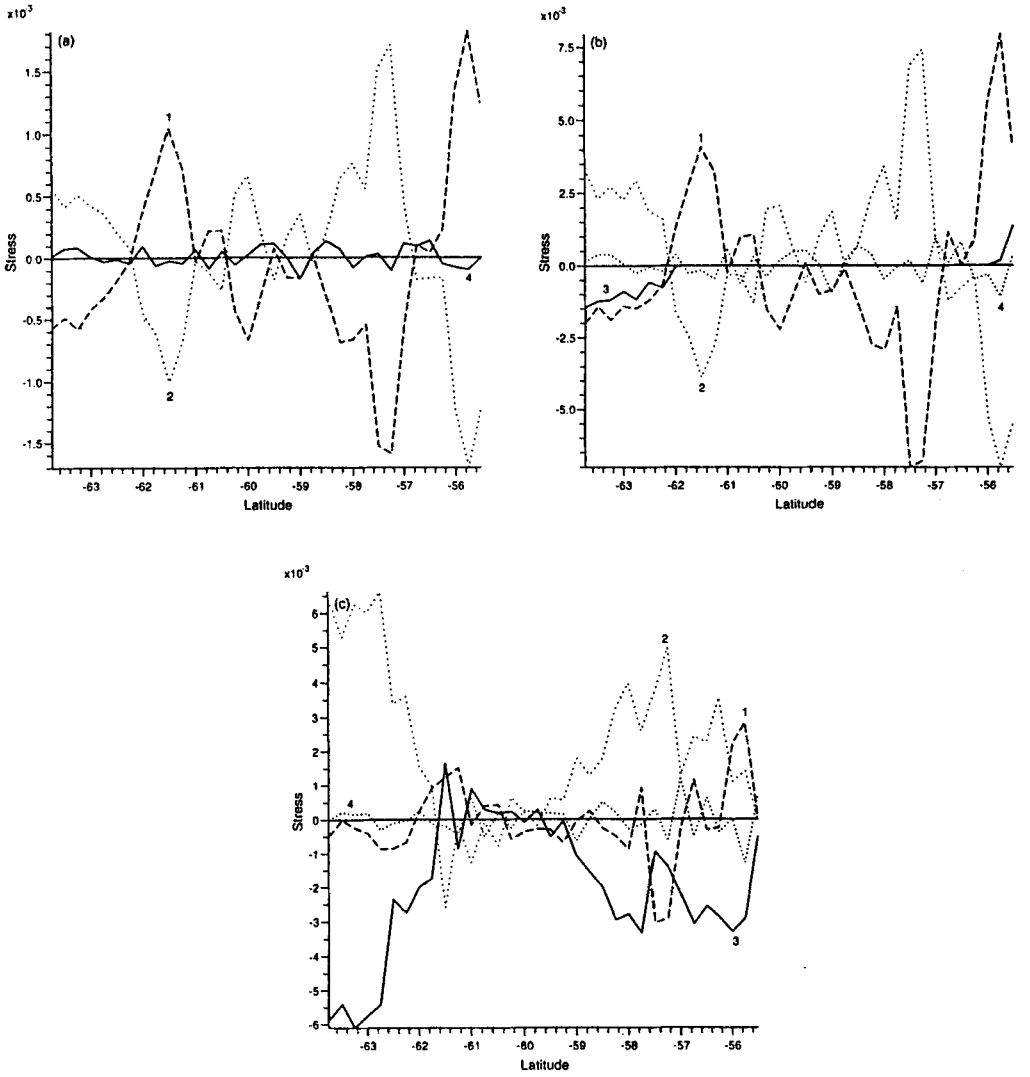


Figure 6. The time and zonally averaged momentum balance at intermediate levels. (a) The balance between levels 3 and 6 (44–185.5 m), (b) the balance between levels 7 and 13 (185.5–1190 m), and (c) the balance between levels 14 and 17 (1190–2056 m). Lines 1, 2, 3 and 4 represent the divergence of Reynolds stress, Coriolis, pressure, and remaining (small) terms respectively. The units of stress are N $m^{-2}$.

layers and above topographic obstacles. This balance indicates that the meridional eddy flux of potential vorticity is zero (Marshall *et al.* 1993). That is, the poleward flux of relative vorticity balances the poleward ageostrophic flux of planetary vorticity. Again the terms in the balance here are much smaller in magnitude than those in the surface and deep-level balances. Consequently the meridional transport in this layer is an order of magnitude smaller than that in the surface Ekman layer or in the deep levels where there are topographic obstacles.

From the base of level 6 to the base of level 13 ($h_{13} = 1190$ m) obstructions appear at the south of the ACCB. These are visible in Fig. 2(b). The balance (Fig. 6(b)) between

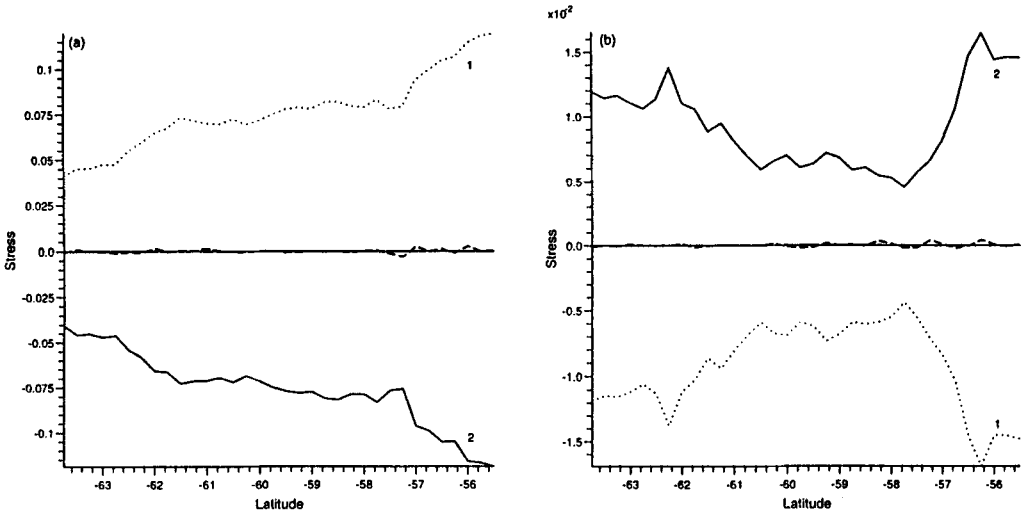


Figure 7. The time and zonally averaged momentum balance at deep levels. (a) The balance between levels 18 and 25 (2056–3874 m), and (b) the balance between levels 26 and 32 (3874–5499 m). Lines 1 and 2 represent the Coriolis and pressure terms respectively. The units of stress are N m$^{-2}$.

these levels is

$$\rho_0\overline{\left[\int_{-h_{13}}^{-h_6}\frac{1}{a\cos\phi}\frac{\partial}{\partial\phi}(uv\cos\phi)\,\mathrm{d}z\right]}-\rho_0\overline{\left[\int_{-h_{13}}^{-h_6}fv\,\mathrm{d}z\right]}=-\frac{1}{a\cos\phi}\overline{\left[\int_{-h_{13}}^{-h_6}\frac{\partial p}{\partial\lambda}\,\mathrm{d}z\right]}. \tag{13}$$

The overall structure here is much the same as Fig. 6(a). Once more the main balance is between the poleward momentum-flux divergence and the Coriolis term. The main difference is a small contribution from the pressure term, as topography starts to intrude into the ACCB.

From the base of level 13 to the base of level 17 ($h_{17} = 2056$ m) more and more of the ACCB becomes obstructed. The main terms in the zonal momentum balance are the same as those in (13). However, the pressure term begins to balance the Coriolis term (Fig. 6(c)) as much more of the ACCB is blocked at these depths.

### (*c*) *The deep levels*

At depths greater than 2056 m the main marine ridges obstruct the ACCB. The balance from this point to the base of level 25 ($h_{25} = 3874$ m) is

$$-\rho_0\overline{\left[\int_{-h_{25}}^{-h_{17}}fv\,\mathrm{d}z\right]}=-\frac{1}{a\cos\phi}\overline{\left[\int_{-h_{25}}^{-h_{17}}\frac{\partial p}{\partial\lambda}\,\mathrm{d}z\right]}. \tag{14}$$

Figure 7(a) illustrates this balance. There are southward-flowing deep currents associated with pressure differences across the major topographic ridges. That is the topographic form stress. The magnitude of the terms in the balance here is the same order as those in the surface balance (10). The southward transport between these levels balances the northward Ekman flux at the surface, just as the stress produced by the topography at these levels balances that input by the wind at the surface.

At the very deepest levels (26–32, 3874–5499 m) the balance is between the same two terms. However, the direction of topographic stress reverses and actually accelerates the eastward flow, as is seen in Fig. 7(b). Killworth and Nanneh (1994) also noticed sign

changes in the interfacial form stress at the deepest layers. This reversal in the stress is associated with a westward bottom flow and the northwards flow of Antarctic bottom water. However, the northwards transport and the corresponding stress are an order of magnitude smaller than the southward transport and corresponding stress in levels 18–25.

### (*d*) *The vertical structure of momentum input to the ACCB*

The ACCB has open northern and southern boundaries and therefore the Reynolds stresses are non zero on these boundaries. This is in contrast to many idealized studies, for example Wolff *et al.* (1991). Integrating the zonal momentum equation (1) with respect to latitude from $\phi_A$ (the southern boundary of the ACCB) to $\phi_B$ (the northern boundary of the ACCB) gives

$$\rho_0 \frac{\partial}{\partial t} \int_{\phi_A}^{\phi_B} a\overline{[u]}\mathrm{d}\phi$$

$$= \rho_0 \int_{\phi_A}^{\phi_B} af\overline{[v]}\mathrm{d}\phi - \rho_0(\overline{[u_*\, v_*]}|_{\phi_B} - \overline{[u_*\, v_*]}|_{\phi_A}) - \rho_0(\overline{[u'v']}|_{\phi_B} - \overline{[u'v']}|_{\phi_A})$$

$$+ \int_{\phi_A}^{\phi_B} \overline{[Q]}\mathrm{d}\phi, \tag{15}$$

where $Q$ is the sum of the remaining terms. Below the wind-driven surface layer and above the topography $Q$ is small.

The redistribution of zonal momentum in the ACCB by eddies is a sink of the zonal momentum (see Fig. 8). The input of the standing eddies (the second term on the right-hand side of (15)) is bigger than that of the transient eddies (the third term on right-hand side of (15)). The contribution of Reynolds stresses to the depth-averaged zonal momentum balance is met almost entirely by the motion in the top 2000 m of the ACCB. The standing eddies are effectively a dragging factor and transient eddies a forcing factor (see Fig. 8). It is well known from studies using quasi-geostrophic models (McWilliams *et al.* 1978) that transient eddies concentrate momentum into jets. Furthermore, Morrow *et al.* (1992) have shown, using GEOSAT data, that transient eddies at the ocean surface provide a net acceleration to the ACC.

### (*e*) *The zonally averaged meridional circulation*

The eastward wind stress causes a northward Ekman transport. At northerly latitudes (which occur outside of the zonally unbounded region and thus this analysis) the wind stress reduces to zero. At these latitudes the water sinks, in a zonally averaged sense, and returns southward at depth. The circulation is completed by the deep water returning to the surface in the region of the ACCB. Johnson and Bryden (1989) considered this possibility but discounted it. However, in FRAM (see Fig. 2(b)) and other models such a circulation (the Deacon Cell) does exist. Indeed in a zonally averaged sense the Deacon Cell must exist in FRAM, given the set of equations and boundary conditions which are solved. However, this does not mean that such a circulation can be observed in any particular meridional plane. Döös and Webb (1994) have made a thorough examination of the Deacon Cell in FRAM and showed that the cell virtually vanishes when the meridional circulation is plotted as a function of latitude and density. This is because the cell arises from differences in the depth of density surfaces between western boundary currents and recirculating interior flow. Water flowing on each density surface produces a meridional cell which extends a few hundred metres in the vertical. When a number of these cells are

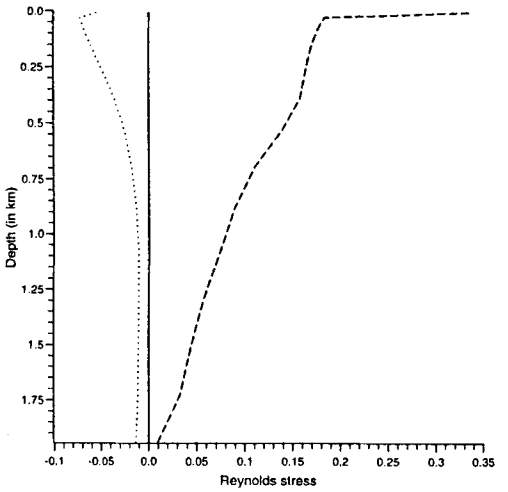


Figure 8. The input of the momentum into the Antarctic Circumpolar Current belt with depth, by standing eddies (the second term on the right-hand side of (15), dashed line) and by transient eddies (the third term on the right-hand side of (15), dotted line). The units of stress are N $m^{-2}$.

combined a single cell is produced which extends from the surface to 2000 m in depth. Thus the Deacon Cell is produced by a circulation in which water particles do not change their density.

## 5. The vertical transfer of momentum

The mechanism by which the momentum input at the surface (by the wind) is transferred down the water column is of great importance. Studies with quasi-geostrophic models (McWilliams *et al.* 1978; Wolff *et al.* 1991) suggest that this process is achieved by interfacial form stress, that is, by the current moving over an undulating density surface. Here, higher (lower) pressure would be found on the upstream (downstream) side of a rise (fall) in the height of a denisty surface. In a level-coordinate model such as FRAM it is difficult (although not impossible (Killworth and Nanneh 1994)) to diagnose this physical process. However, it is straightforward (as shown later) to relate the interfacial form stress to a meridional density (heat) flux. In fact it is interesting to note that temperature (rather than salinity) plays a dominant role here. The following calculations have been repeated with temperature replacing density, giving similar results. The calculations in sections 3 and 4 were performed as the model was running. Whereas the calculations in this section were computed retrospectively and are based on 72 monthly data-sets from the final six years of the FRAM 16-year run. It is unlikely that there is a significant short time-scale contribution missing as the temperature-flux calculation (mentioned above) was available for both daily and monthly data with negligible differences.

### (*a*) *An extension of the Johnson–Bryden theory*

Here it is assumed that the density $\rho$ satisfies the tracer equation (5). This would be exactly true if the equation of state (6) were linear. Furthermore we neglect diffusion and diabatic forcing, and take a quasi-geostrophic approach (but only over the relatively narrow ACCB). It is tempting to take the quasi-geostrophic approximation from the coast of Antarctica up to and including the ACCB. However, a glimpse at any atlas of climatological data (Levitus 1982; Olbers *et al.* 1992) shows this is not wise as there are large changes

in the background stratification. With these approximations the equation (5) for density conservation becomes

$$\frac{\partial \rho}{\partial t} + \frac{1}{a \cos\phi}\frac{\partial}{\partial \lambda}(u\rho) + \frac{1}{a\cos\phi}\frac{\partial}{\partial \phi}(v\rho\cos\phi) + w\frac{\partial}{\partial z}(\overline{[\rho]}) = 0. \tag{16}$$

Now taking the zonal and time average we obtain

$$\overline{[w]} = -\frac{1}{a\cos\phi}\frac{\partial}{\partial\phi}\left(\frac{\overline{[v\rho]}\cos\phi}{\overline{[\rho]}_z}\right). \tag{17}$$

The vertical velocity at the base of the Ekman layer is given by Ekman pumping. In the time and zonal average this is

$$\overline{[w]} = -\frac{1}{a\cos\phi\rho_0 f_0}\frac{\partial(\overline{[\tau_s^\lambda]}\cos\phi)}{\partial\phi}, \quad \text{at} \quad z = -h_E, \tag{18}$$

where $f_0$ is the average Coriolis parameter for the ACCB. From (17) and (18) we have

$$\frac{\partial}{\partial\phi}\left(\frac{\overline{[v\rho]}\cos\phi}{\overline{[\rho]}_z}\right) = \frac{1}{\rho_0 f_0}\frac{\partial(\overline{[\tau_s^\lambda]}\cos\phi)}{\partial\phi}, \quad z = -h_E. \tag{19}$$

Integrating (19) gives

$$\rho_0 f_0 \frac{\overline{[v\rho]}}{\overline{[\rho]}_z} = \overline{[\tau_s^\lambda]} + C_1, \quad z = -h_E, \tag{20}$$

where $C_1$ is a constant of integration.

Eliminating $w$ from (17) using the time and zonally averaged form of the continuity equation (4), we obtain

$$\frac{\partial}{\partial\phi}\left\{\frac{\partial}{\partial z}\left(\frac{\overline{[v\rho]}}{\overline{[\rho]}_z}\cos\phi\right)\right\} = \frac{\partial(\overline{[v]}\cos\phi)}{\partial\phi}. \tag{21}$$

After integrating with respect to $\phi$ we may write

$$\frac{\partial}{\partial z}\left(f_0\frac{\overline{[v\rho]}}{\overline{[\rho]}_z}\right) = f_0\overline{[v]} + C_2(z), \tag{22}$$

where $C_2(z)$ is a function, dependent only on the vertical coordinate $z$. At this stage it should be noted that if we had taken the quasi-geostrophic approximation to be valid from the coast of Antarctica to the ACCB (Marshall *et al.* 1993) then we would have obtained $C_2(z) = 0$. Evaluating the first two terms of (22) in FRAM shows that $|f_0\overline{[v]}| \ll |C_2(z)|$ and $\overline{[v][\rho]} \ll \overline{[v\rho]}$. Thus integrating (22) from the base of the Ekman layer to a depth $z$ and using (20) gives

$$\rho_0 f_0 \frac{\overline{[\hat{v}\hat{\rho}]}}{\overline{[\rho]}_z} = \overline{[\tau_s^\lambda]} + C(z). \tag{23}$$

Here $C(z)$ is dependent on $C_1$ and $C_2(z)$ and $\hat{}$ denotes a deviation from the time and zonal mean ($\hat{\mu} = \mu - \overline{[\mu]}$).

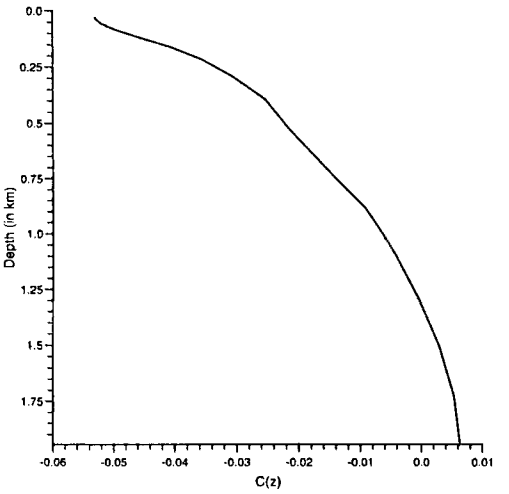


Figure 9. The function $C(z)$ (see text), in units of N m$^{-2}$, plotted as a function of depth.

Many of the theoretical investigations and numerical models of the circulation in the Southern Ocean describe the dynamics in a zonal channel with solid meridional boundaries. Usually $\tau_s^\lambda$ becomes zero at the boundaries, and coupled with no-flow boundary conditions the meridional velocity component also reduces to zero. In this case $C(z) = 0$. Johnson and Bryden (1989) also write (23) with $C(z) = 0$.

The profile of $C(z)$, calculated as a residual of (23) in FRAM, can be seen in Fig. 9. The relationship (23) allows us to understand the large difference between

$$\rho_0 f_0 \frac{\overline{[\hat{v}\hat{\rho}]}}{\overline{[\rho]}_z} \quad \text{and} \quad \overline{[\tau_s^\lambda]}$$

in the upper layers (see Fig. 10), where the neighbouring oceans have a large effect on the meridional heat, salt and density fluxes. The function $C(z)$ can either be set by the conditions to the north or south of the ACCB. In the case of the south, it is defined by the diabatic forcing and the deviation from the quasi-geostrophic approximation between the ACCB and the Antarctic coast. Immediately below the Ekman layer, $C = -0.053$ N m$^{-2}$. It is interesting that $|C(z)|$ reduces with depth, and below a depth of 1000 m it is relatively small. This can be seen in Fig. 10, where the left-hand side of (23) is almost equal to the zonally averaged eastward wind stress for the five levels between 1000 and 2000 m.

### (*b*) *Eliassen–Palm theory*

In order to gain a clearer physical understanding of the function $C(z)$ we use Eliassen–Palm vectors and cross-sections. This approach, which first appeared in meteorology, is a powerful method for diagnosing the influence of eddies on the zonal mean flow (Eliassen and Palm 1961; Andrews and McIntyre 1976; Edmon *et al.* 1980). The main idea is to use a transformation of the hydrodynamic equations for the zonal flow. The influence of eddies only occurs in the zonal momentum equation

$$\frac{\partial [u]}{\partial t} - f[v_r] - \mathcal{F} = \nabla . \mathbf{I}, \tag{24}$$

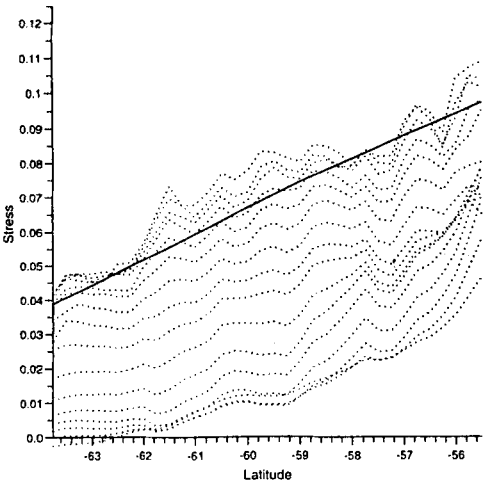


Figure 10. A comparison between the scaled eddy density flux (interfacial form stress) $\rho_0 f_0 \overline{[\hat{v}\hat{\rho}]}/\overline{[\rho]}_z$ at levels 2–17 (dotted lines) and the zonal and time averaged eastward wind stress $\overline{[\tau_s^{\lambda}]}$ (solid line). The magnitude of the form stress increases with depth. Between levels 13–17 (1000–2000 m) the form stress approximately equals the wind stress. The units are N m$^{-2}$.

as the divergence of the Eliassen–Palm vector **I** where

$$\mathbf{I} = (I_\phi, I_z) = \left(-[u_* v_*], f\frac{[v_*\rho_*]}{[\rho]_z}\right). \tag{25}$$

It should be noted that $\nabla.\mathbf{I}$ is the meridional flux of potential vorticity. The term $\mathcal{F}$, which includes friction and vertical advection, is small (above topography and below the wind-driven surface layer). The horizontal component $I_\phi$ is the Reynolds stress and the vertical component $I_z$ is connected with the interfacial form stress (see (23)). Thus the eddies drive the zonal flow by Reynolds stresses and density fluxes.

A complete set of equations can be written for $[u]$, $[\rho]$ and the so-called 'residual meridional circulation' with components $[v_r]$, $[w_r]$, where

$$[v_r] = [v] - \frac{\partial}{\partial z}\left(\frac{[v_*\rho_*]}{[\rho]_z}\right), \tag{26}$$

$$[w_r] = [w] + \frac{1}{a\cos\phi}\frac{\partial}{\partial\phi}\left(\frac{[v_*\rho_*]\cos\phi}{[\rho]_z}\right). \tag{27}$$

The residual meridional circulation is induced by eddies as the divergence of the Eliassen–Palm vector (Edmon *et al.* 1980). Marshall *et al.* (1993) use (26) with $[v_r] = 0$, which is a consequence of their model formulation allowing the elimination of $C(z)$ (as noted in section (*a*)).

Figure 11 illustrates the time-mean Eliassen–Palm vectors and their divergence in the ACCB. It can be seen from Figs. 10 and 11(a) that the vertical component of the Eliassen–Palm vector is almost everywhere upward, that is

$$I_z = f\frac{\overline{[\hat{v}\hat{\rho}]}}{[\rho]_z} \geqslant 0. \tag{28}$$

This implies that the density flux $\overline{[\hat{v}\hat{\rho}]}$ is positive. Thus, on average at a particular level, higher-density water should flow northward and lower-density water southward. The zon-

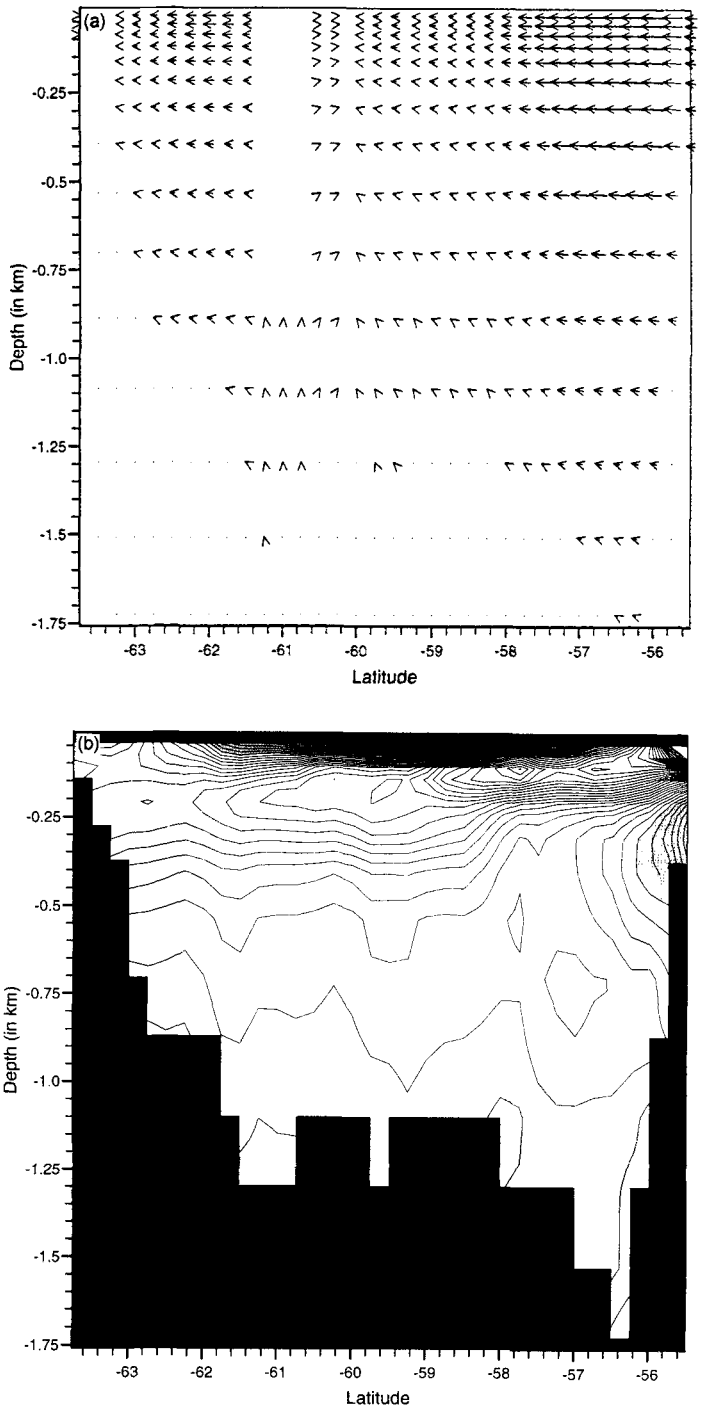


Figure 11. (a) The Eliassen–Palm vectors in the Antarctic Circumpolar Current belt. The horizontal distance between grid points is equal to a magnitude of $10^{-3}$ $m^2s^{-2}$. Vectors smaller than $5 \times 10^{-5}$ $m^2s^{-2}$ are not plotted. (b) The divergence of the Eliassen–Palm vector in the ACCB. The contour interval is $10^{-8}$ $m\,s^{-2}$ and positive regions are shaded.

ally averaged current in the ACCB is everywhere eastward above the level of topographic obstacles, which suggests penetration of eastward momentum with depth and requires $I_z > 0$ (as noted above). This can be seen in Fig. 11(a), which illustrates the time-mean Eliassen–Palm vectors, although it is more clear with reference to Fig. 10. There is a northward flux of eastward momentum almost everywhere. Only between 60°S–61°S does this flux reverse and then its magnitude is very small. The tilt of the Eliassen–Palm vectors increases with depth, as the momentum flux is reduced and the density flux increases.

The physical sense of the function $C(z)$ can be interpreted by considering the residual meridional circulation. From (23) we may write

$$\frac{\mathrm{d}C(z)}{\mathrm{d}z} = \frac{\partial}{\partial z}\left(\rho_0 f_0 \frac{\overline{[\hat{v}\hat{\rho}]}}{\overline{[\rho]}_z}\right), \tag{29}$$

and therefore (26) gives

$$\overline{[v_r]} = \overline{[v]} - \frac{1}{\rho_0 f_0}\frac{\mathrm{d}C}{\mathrm{d}z}. \tag{30}$$

As noted earlier, output from FRAM shows that in the ACCB $\overline{[v]}$ is at least one order of magnitude smaller than

$$\frac{1}{\rho_0 f_0}\frac{\mathrm{d}C}{\mathrm{d}z}.$$

Thus (30) gives

$$\overline{[v_r]} = -\frac{1}{\rho_0 f_0}\frac{\mathrm{d}C}{\mathrm{d}z}. \tag{31}$$

Furthermore, the divergence of the Eliassen–Palm vector, illustrated in Fig. 11(b), is dominated by $I_z$. This is because the scale of $I_\phi$ is larger than $I_z$, especially in the upper layers. Thus with reference to (26) the figure can also be interpreted as contours of $\overline{[v_r]}$. Note, that $\overline{[v_r]} < 0$ should be true everywhere, that is the residual circulation is directed toward the pole. However in FRAM there are some near-surface regions of static instability which invalidate the approximations that have been made.

From (31) the function $C(z)$ can be written as

$$C(z) = \rho_0 f_0 \overline{[\psi_r]}, \tag{32}$$

where $\overline{[\psi_r]}$ is the stream function for the steady-state residual circulation. Thus the stream function should be parallel horizontal lines, which Fig. 11(b) suggests is approximately true. Finally substituting $C(z)$ in (23) we can write

$$\overline{[\tau_s^\lambda]} = \rho_0 f_0 \frac{\overline{[\hat{v}\hat{\rho}]}}{\overline{[\rho]}_z} - \rho_0 f_0 \overline{[\psi_r]}. \tag{33}$$

Thus above the level of topographic obstacles the wind stress is balanced by the form stress and a term proportional to the stream function of the residual circulation. This second term arises as a response to the eddy induced torque on the zonal mean flow (Edmon *et al.* 1980).

### (c) *The contribution of standing and eddy motions*

The left-hand side of (23) can be separated into standing and transient eddy terms

$$\rho_0 f_0 \frac{\overline{[\hat{v}\hat{\rho}]}}{\overline{[\rho]}_z} = \rho_0 f_0 \frac{\overline{[v_*\rho_*]}}{\overline{[\rho]}_z} + \rho_0 f_0 \frac{\overline{[v'\rho']}}{\overline{[\rho]}_z}. \tag{34}$$

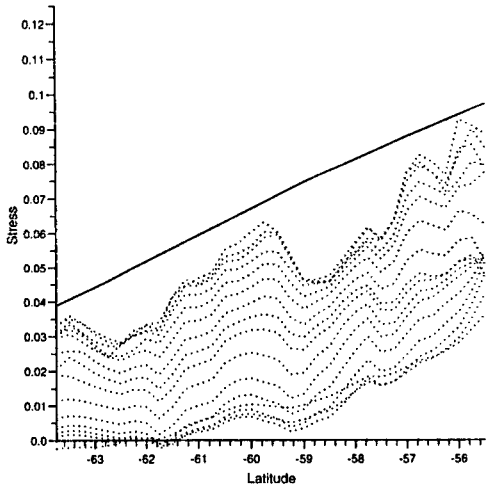


Figure 12. A comparison between the scaled standing-eddy density flux (form stress due to standing eddies) $\rho_0 f_0 [\bar{v}_* \overline{\rho_*}]/[\overline{\rho}]_z$ at levels $k$=2–17 (dotted lines) and the zonal and time averaged eastward wind stress $[\overline{\tau_S^x}]$ (solid line). The magnitude of the standing eddy form stress increases with depth. The units are N m$^{-2}$.

The first term on the right-hand side describes the eddy density flux by standing eddies, and is illustrated in Fig. 12. It is created by the meridional displacement of the mean path of the ACC. The displacement is mainly due to topographic features (see Fig. 1). The contribution from standing eddies provides most of the density flux. Comparing Figs. 10 and 12 it is possible to see the contribution from transient eddies. This depends upon synoptic eddies, created mainly by baroclinic instability of the large-scale current. Although the contribution from transient eddies is smaller, there are two latitudes, at 62.5°S and 58.5°S, where they provide more than one third of the density flux associated with the penetration of wind stress. It should be noted that by averaging along a path which in some sense follows the ACC (rather than a latitude circle) it is possible to reduce the contribution from standing eddies (Marshall *et al.* 1993; Ivchenko *et al.* 1996).

## 6. Discussion

McWilliams *et al.* (1978), Treguier and McWilliams (1990) and Wolff *et al.* (1991) have investigated the dynamics of channel flows. Their models have shown the importance of topographic obstacles in the zonal momentum balance and also that synoptic eddies play an important role. Reynolds stresses, due to transient eddies, redistribute momentum and as a result the main jet increases in strength while currents on the periphery become weaker. These models have indicated that eddies play an important role in the downward momentum transfer and that the main sink of zonal momentum in the lower layers is topographic form stress or (for flat-bottom experiments) bottom friction. However, are the results from zonal channel-flow models applicable to the ACCB in the Southern Ocean? The ACCB does not have solid boundaries on its northern and southern edges, the averaged zonal wind stress is not zero on these open boundaries, and there is also interaction between the ACCB and neighbouring areas.

The analysis presented here, along with the isopycnal momentum budget of Killworth and Nanneh (1994), confirms the importance of the interfacial form stress in the transfer of zonal momentum downwards. The penetration of the zonal momentum is connected with meridional density fluxes. The residual meridional circulation depends upon the boundary

conditions to the north or south of the ACCB. In channel models with vertical walls the function $C(z)$, of (23), should be zero and the formula of Johnson and Bryden (1989) is correct. This has been demonstrated in a primitive-equation model of a simple channel with idealized topography (to be reported elsewhere). However, the residual circulation in the ACCB is principally horizontal and poleward. The function $C(z)$ is proportional to the stream function of the residual meridional circulation and is thus non zero. The contribution of standing eddies is larger than the transients. Standing eddies appear because the ACC is steered northward and southward by the topography (see Fig. 1). Thus, the topographic relief in the ACCB area is an important factor for the vertical penetration of wind stress.

In the surface layer there is a northward Ekman flux, the total meridional transport in this layer is 7–17 Sverdrups. This transport depends on latitude, increasing almost linearly as it flows equatorward. In the main ACCB layer the Reynolds divergence is balanced by the Coriolis force, connected with ageostrophic meridional mass flux. The standing eddy contribution to Reynolds stresses is larger than the transient eddy contribution. The meridional transport in this layer is much less than the Ekman flux in the surface layer. The main sink of zonal momentum is in the lower layer, through topographic form stress. The meridional flux here balances the Ekman flux in the surface layer.

## Acknowledgements

This work would not have been possible without the help of many members of the FRAM group, in particular David Webb, Kelvin Richards, John Johnson, Peter Killworth, Bablu Sinha, Beverly de Cuevas, Neil Wells, Andrew Coward and Steve Maskell. We are also grateful for the helpful comments of Dirk Olbers, John Marshall and two anonymous referees. Financial support was provided by the Natural Environment Research Council grants GST/02/407 and GST/02/408.

## References

Andrews, D. G. and McIntyre, M. E. 1976 Planetary waves in horizontal and vertical shear: the generalized Eliassen–Palm relation and the mean zonal acceleration. *J. Atmos. Sci.*, **33**, 2031–2048

Bryan, K. and Cox, M. D. 1972 The circulation in the world ocean: A numerical study, I, A homogeneous model. *J. Phys. Oceanogr.*, **2**, 319–335

Bryan, K., Manabe, S. and Pacanowski, R. C. 1975 A global ocean–atmosphere climate model. II: The oceanic circulation. *J. Phys. Oceanogr.*, **5**, 30–46

Bye, J. A. T and Sag, T. W. 1972 A numerical model for the circulation in a homogeneous world ocean. *J. Phys. Oceanogr.*, **2**, 305–318

Cox, M. D. 1975 'A baroclinic numerical model of the world ocean: Preliminary results'. Pp. 107–120, in Numerical models of ocean circulation. National Academy of Sciences, Washington, DC

1984 'A primitive equation, 3-dimensional model of the ocean'. GFDL Ocean Group Tech. Rep. No. 1

1990 An idealized model of the world ocean. Part I: The global-scale water masses. *J. Phys. Oceanogr.*, **20**, 1730–1752

Danabasoglu, G., McWilliams, J. C. and Gent, P. R. 1994 The role of mesoscale tracer transports in the global ocean circulation. *Science*, **264**, 1123–1126

Döös, K. and Webb, D. J. 1994 The Deacon Cell and the other meridional cells in the Southern Ocean. *J. Phys. Oceanogr.*, **24**, 429–442

Edmon, H. J., Hoskins, B. J. and McIntyre, M. E. 1980 Eliassen–Palm cross sections for the troposphere. *J. Atmos. Sci.*, **37**, 2600–2616

Eliassen, A. and Palm, E. 1961 On the transfer of energy in stationary mountain waves. *Geofys. Publ.*, **22**, No. 3, 1–23

Gill, A. E. and Bryan, K. 1971 Effects of geometry on the circulation of a three-dimensional southern-hemisphere ocean model. *Deep Sea Res.*, **18**, 685–721

Gordon, A. L., Molinelli, E. and Baker, T. 1982 *Southern ocean atlas*. Columbia University Press

Grose, T. J. 1992 'Analysis of theoretical and observational techniques using the Fine-Resolution Antarctic Model'. University of East Anglia thesis, Norwich, UK

Hellerman, S. and Rosenstein, M. 1983 Normal monthly wind stress over the world ocean with error estimates. *J. Phys. Oceanogr.*, **13,** 1093–1104

Ivchenko, V. O., Richards, K. J. and Stevens, D. P. 1996 The dynamics of the Antarctic Circumpolar Current. *J. Phys. Oceanogr.*, **26,** 753–774

Johnson, G. C. and Bryden, H. L. 1989 On the size of the Antarctic Circumpolar Current. *Deep Sea Res.*, **36,** 39–53

Killworth, P. D. 1992 An equivalent-barotropic mode in FRAM. *J. Phys. Oceanogr.*, **22,** 1379–1387

Killworth, P. D. and Nanneh, M. M. 1994 On the isopycnal momentum budget of the Antarctic Circumpolar Current in the Fine-Resolution Antarctic Model. *J. Phys. Oceanogr.*, **24,** 1201–1223

Levitus, S. 1982 'Climatological atlas of the world ocean'. NOAA Prof. Pap. 13, US Dept. of Commerce

Manabe, S., Bryan, K. and Spelman, M. J. 1990 Transient response of a global ocean-atmosphere model to a doubling of atmospheric carbon dioxide. *J. Phys. Oceanogr.*, **20,** 722–749

Marshall, D. 1995 Topographic steering of the Antarctic Circumpolar Current. *J. Phys. Oceanogr.*, **25,** 1636–1650

Marshall, J., Olbers, D., Ross, H. and Wolf-Gladrow, D. 1993 Potential vorticity constraints on the dynamics and hydrography of the Southern Ocean. *J. Phys. Oceanogr.*, **23,** 465–487

McWilliams, J. C. and Chow, J. S. 1981 Equilibrium geostrophic turbulence. I: A reference solution in a beta plane channel. *J. Phys. Oceanogr.*, **11,** 921–949

McWilliams, J. C., Holland, W. R. and Chow, J. S. 1978 A description of numerical Antarctic Circumpolar Currents. *Dyn. Atmos. Oceans.*, **2,** 213–291

Morrow, R., Church, J., Coleman, R., Chelton, D. and White, N. 1992 Eddy momentum flux and its contribution to the Southern Ocean momentum balance. *Nature*, **357,** 482–484

Munk, W. H. and Palmén, E. 1951 Note on the dynamics of the Antarctic Circumpolar Current. *Tellus*, **3,** 53–55

Nowlin Jr, W. D. and Klinck, J. M. 1986 The physics of the Antarctic Circumpolar Current. *Rev. Geophys.*, **24,** 469–491

Olbers, D. and Wenzel, M. 1990 Determining diffusivities from hydrographic data by inverse methods with applications to the circumpolar current. In *Ocean circulation models: Combining data and dynamics*. Eds. J. Willebrand and D. L. T. Anderson. Kluwer Academic Publishers, Dordrect, Holland

Olbers, D. and Wübber, C. 1991 The role of wind and buoyancy forcing of the Antarctic Circumpolar Current. Pp. 161-192 In *Strategies for future climate research*, Ed. M. Latif. Max-Planck-Institut fur Meteorologie, Hamburg, Germany

Olbers, D., Gouretski, V., Seiss, G. and Schröter, J. 1992 *Hydrographic atlas of the Southern Ocean*. Alfred Wegener Institute, Bremerhaven, Germany

Saunders, P. M. and Thompson, S. R. 1993 Transport, heat and freshwater fluxes within a diagnostic numerical model (FRAM). *J. Phys. Oceanogr.*, **23,** 452–464

Semtner, A. J. and Chervin, R. M. 1988 A simulation of the global ocean circulation with resolved eddies. *J. Geophys. Res.*, **93,** 15502–15522

1992 Ocean general circulation from a global eddy-resolving model. *J. Geophys. Res.*, **97,** 5493–5550

Stevens, D. P. and Killworth, P. D. 1992 The distribution of kinetic energy in the Southern Ocean: a comparison between observations and an eddy-resolving general circulation model. *Phil. Trans. R. Soc. London* **B 338,** 251–257

The FRAM group 1991 Initial results from a fine-resolution model of the Southern Ocean. *EOS, Trans. Am. Geophys. Union*, **72,** 169, 174–175

Treguier, A. M. and McWilliams, J. C. 1990 Topographic influences on wind-driven, stratified flow in a $\beta$-plane channel: an idealized model for the Antarctic Circumpolar Current. *J. Phys. Oceanogr.*, **20,** 321–343

Webb, D. J., Killworth, P. D., Coward, A. C. and Thompson, S. R. 1991 *'The FRAM atlas of the Southern Ocean'*. Natural Environment Research Council, Swindon, UK

Wells, N. C. and deCuevas, B. A. 1995 Depth-integrated vorticity budget of the Southern Ocean from a general circulation model. *J. Phys. Oceanogr.*, **25,** 2569–2582

Wolff, J.-O., Olbers, D. and Maier-Reimer, E. 1991 Wind-driven flow over topography in a zonal $\beta$-plane channel: A quasi-geostrophic model of the Antarctic Circumpolar Current. *J. Phys. Oceanogr.*, **21,** 236–264